Constraints on dust production in the Edgeworth-Kuiper Belt from Pioneer 10 and New Horizons measurements

Dong Han,[1] Andrew R. Poppe,[2] Marcus Piquette,[1] Eberhard Grün,[1] and Mihály Horányi[1,3]

Received 24 October 2011; revised 10 November 2011; accepted 13 November 2011; published 28 December 2011.

[1] Impact ejecta and collisional debris from the Edgeworth-Kuiper Belt are the dominant source of micron-sized grains in the outer solar system, as they slowly migrate inwards through the outer solar system before most grains are ejected during close encounters with Jupiter. These grains drive several phenomena in the outer solar system, including the generation of impact ejecta clouds at airless bodies, the formation of ionospheric layers and neutral gases in the atmospheres of the giant planets due to meteoric ablation, the generation of tenuous outer planetary ring systems and the spatial and compositional alteration of Saturn's main rings. Previous analyses have offered estimates of the net mass production rate from the Edgeworth-Kuiper Belt both theoretically and observationally. In order to improve upon these estimates, we compare measurements of the interplanetary dust density in the outer solar system by both the Pioneer 10 meteoroid detector and the New Horizons Student Dust Counter with a dynamical dust grain tracing model. Our best estimates for the net mass production rate and the ejecta mass distribution power law exponent are $(8.9 \pm 0.5) \times 10^5$ g/s and 3.02 ± 0.04, respectively. **Citation:** Han, D., A. R. Poppe, M. Piquette, E. Grün, and M. Horányi (2011), Constraints on dust production in the Edgeworth-Kuiper Belt from Pioneer 10 and New Horizons measurements, *Geophys. Res. Lett.*, *38*, L24102, doi:10.1029/2011GL050136.

1. Introduction

[2] Since the first trans-Neptunian object was discovered in 1992, more than 1,100 similar objects have been found in the Edgeworth-Kuiper Belt (EKB), between 30 and 50 AU [*Jewitt and Luu*, 1995; *Luu and Jewitt*, 2002; *Kavelaars et al.*, 2009]. While other objects, such as Jupiter Family Comets, can contribute dust to the outer solar system [*Nesvorný et al.*, 2010], previous work has suggested that EKBOs represent the dominant source of micron-sized dust grains in the outer solar system, due to both mutual collisions and secondary production by interstellar grain bombardment [*Stern*, 1996; *Yamamoto and Mukai*, 1998]. For EKB grains with radius, $0.1 < a_d < 10$ μm, these processes are estimated to produce between 8.6×10^4 and 2.9×10^7 g/s for mutual collisions and between 3.7×10^5 and 2.4×10^6 g/s for interstellar grain bombardment. The migration of these grains into the solar system under the influence of gravity, solar radiation pressure, solar wind drag, and the electromagnetic Lorentz force creates a debris disk from the orbit of Jupiter out to approximately 50 AU, and potentially further, and has been previously modeled using a variety of methods [*Liou and Zook*, 1997, 1999; *Moro-Martin and Malhotra*, 2002; *Holmes et al.*, 2003; *Vitense et al.*, 2010; *Kuchner and Stark*, 2010].

[3] An accurate calculation of the mass production rate in the EKB has implications for several processes in the outer solar system, including the formation of impact-generated ejecta clouds around airless bodies [*Thiessenhusen et al.*, 2002; *Krivov et al.*, 2003; *Poppe and Horányi*, 2011], the production of ionospheric layers and neutral gases in the atmospheres of the giant planets and Titan from meteoric ablation [*Moses*, 1992; *Feuchtgruber et al.*, 1997; *Molina-Cuberos et al.*, 2001], the generation of tenuous outer planetary rings [*Colwell and Esposito*, 1990; *Burns et al.*, 1999; *Verbischer et al.*, 2009], and the spatial and compositional evolution of Saturn's main rings [*Northrop and Connerney*, 1987; *Durisen et al.*, 1989, 1992, 1996; *Cuzzi and Estrada*, 1998; *Chambers et al.*, 2008].

[4] In this paper, we present new constraints on the production of micron-sized dust grains in the EKB using measurements of the interplanetary dust density in the outer solar system by both the Pioneer 10 meteoroid detector and the Student Dust Counter (SDC) on the New Horizons mission, combined with a particle-tracing code for EKB-generated dust grains. In Section 2, we describe the particle-tracing code used to establish relative dust grain densities in the outer solar system and present results from the simulation. In Section 3, we use data from Pioneer 10 and SDC to constrain both the total mass production rate and power law index for grains with radii between 0.1 and 10 μm. We summarize the results and discuss their impact in Section 4.

2. Dynamical Dust Grain Model

[5] The motion of micron-sized dust grains in the outer solar system is governed by the gravitational forces from the Sun and the giant planets, solar radiation pressure, solar wind and Poynting-Robertson (PR) drag, and the Lorentz force. For a dust particle with mass, m, and radius, a_d, the equation of motion in a heliocentric inertial frame is,

$$\ddot{\mathbf{r}}_s = -\frac{GM_\odot}{r_s^3}\mathbf{r_s} - \sum_{i=1}^{4}\frac{GM_i}{r_i^3}\mathbf{r_i} + \frac{1}{m}\mathbf{F_L} + \\ + \frac{\pi a_d^2}{mc} SQ_{pr}\left[\left(1-(1+w)\frac{\dot{r}_s}{c}\right)\hat{\mathbf{r}}_\mathbf{s} - (1+w)\frac{\dot{\mathbf{r}}_\mathbf{s}}{c}\right], \quad (1)$$

where $\mathbf{r_s}$ ($\hat{\mathbf{r}}_\mathbf{s}$) is the heliocentric position (unit vector) of the dust particle, $M_\odot$ is the mass of the Sun, M_i is the mass of the

[1]Laboratory for Atmospheric and Space Physics, University of Colorado at Boulder, Boulder, Colorado, USA.
[2]Space Sciences Laboratory, University of California, Berkeley, California, USA.
[3]Department of Physics, University of Colorado at Boulder, Boulder, Colorado, USA.

0094-8276/11/2011GL050136

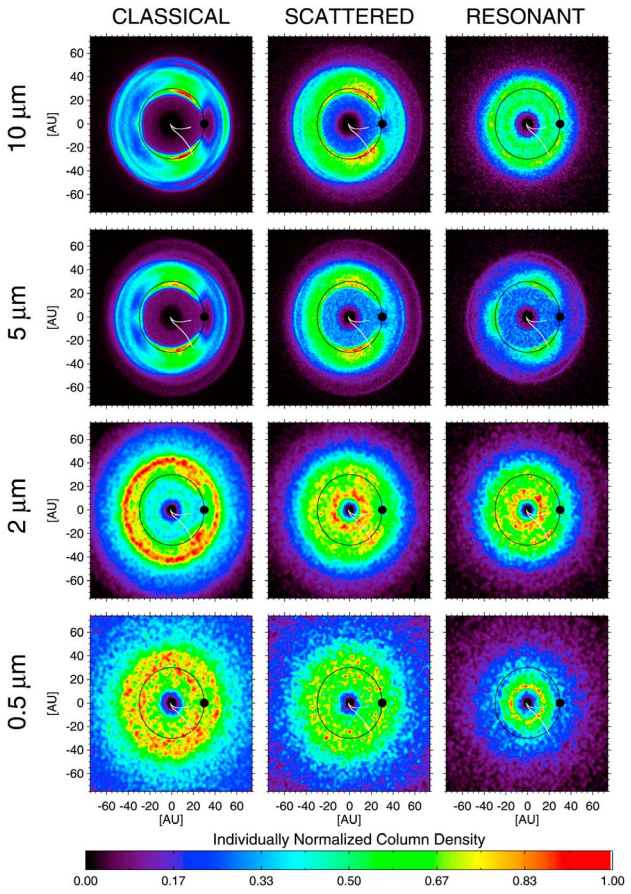

Figure 1. The column density within ±0.5 AU of the ecliptic plane in the Neptune co-rotating frame for four grain radii (0.5, 2.0, 5.0 and 10.0 μm) for three separate initial EKB populations, each normalized to its respective maximum. Noted on each plot is the position and orbit of Neptune. Additionally, the two white lines mark the Pioneer 10 (upper line) and New Horizons (lower line) trajectories.

i^{th} planet, $\mathbf{r_i}$ is the position vector of the dust particle from the i^{th} planet, c and S are the speed of light and the solar radiation flux density, respectively, $Q_{pr} = 1$ is the radiation pressure coefficient, and $w = 0.35$ is the constant ratio between solar wind and PR drags [*Burns et al.*, 1979; *Gustafson*, 1994; *Liou et al.*, 1995]. The Lorentz force is given by $\mathbf{F_L} = q(\dot{\mathbf{r}}_\mathbf{s} \times \mathbf{B})$, where $\mathbf{B}$ is the interplanetary magnetic field as modeled by *Landgraf* [2000], which is based on a Parker spiral while including variations in solar cycle [*Parker*, 1958]. The electrostatic surface potential of the dust particles, independent of their size and distance from the Sun, was set to be a constant $\phi = +5$ volt, resulting in a size dependent charge, $q = 4\pi\epsilon_o a_d \phi$ [*Horányi*, 1996]. Simulations with and without the Lorentz force showed that, as expected from *Landgraf* [2000], the Lorentz force is increasingly important as the grain radius decreases.

[6] Equation (1) was integrated for individual dust grains using a Bulirsch-Stoer step-size controlled integration method [*Press et al.*, 2007]. Particles with radii a_d = [0.5, 1.0, 2.0, …, 9.0, 10.0] μm were integrated, with a total of approximately 10,000 grains for sufficient statistics. Grains were started with orbital elements randomly selected from those typical of three categories of KBOs: Classical, Scattered, and Resonant (Plutino), with each subpopulation comprising 34.7%, 52.1% and 13.2%, respectively [*Kavelaars et al.*, 2009]. While the initial position and velocity of a grain and its parent KBO are identical, the grain's orbit will quickly diverge from its parent's due to the presence of the various perturbing forces listed above. Integration was stopped when a grain arrived near the Sun ($r_s < 0.1$ AU) or left the solar system ($r_s > 200$ AU) with net positive orbital energy.

[7] By keeping track of each grain's position, a relative, statistical equilibrium density map can be calculated for each grain size. The density distribution, $n_a(x, y, z)$, where a denotes the grain size, is constructed on a 150 × 150 × 10 AU grid, by,

$$n_a(x,y,z) = \frac{1}{T_a}\sum_{j=0}^{N_a} t_j(x,y,z), \tag{2}$$

where N_a is the number of grains simulated with radius a_d, T_a is the total time all particles of radius a_d spent in the simulation, and $t_j(x, y, z)$ is the time that the j^{th} particle spent in the 1 × 1 × 1 AU box centered at (x, y, z). In order to highlight the role that mean-motion resonances (MMR) with Neptune play in shaping the equilibrium density, all trajectories are transformed to the Neptune co-rotating frame. Figure 1 shows the equilibrium density of grains for four different sizes (0.5, 2.0, 5.0, and 10.0 μm) within ±0.5 AU of the ecliptic plane for each of the EKB source sub-populations. As expected, larger grains are more often captured in MMRs with Neptune, while smaller grains are more easily scattered and present a more diffuse density distribution [*Liou and Zook*, 1999; *Moro-Martin and Malhotra*, 2002].

3. Model/Data Comparison

3.1. Student Dust Counter and Pioneer 10 Data

[8] To date, the two dedicated measurements of interplanetary dust grain density in the outer solar system come from the Student Dust Counter on the New Horizons mission to Pluto [*Stern*, 2008; *Horányi et al.*, 2008; *Poppe et al.*, 2010] and the meteoroid detector on the Pioneer 10 spacecraft [*Humes*, 1980]. The Pioneer 11 mission also contained a meteoroid detector; however, it did not make measurements outside of 10 AU, which is the approximate heliocentric distance at which EKB grains are expected to be dominant [*Landgraf et al.*, 2002], and therefore, we did not use Pioneer 11 data in our analysis. While of different design, both Pioneer 10 and SDC operated by measuring the cumulative flux of interplanetary grains with radii greater than ≈0.55 μm and ≈3.3 μm (using equation 1 from *Humes* [1980] and assuming a density of $\rho = 2.5$ g/cm^3), respectively. Pioneer 10 made measurements from 1 AU to 18 AU while SDC will eventually make measurements from 2 AU to Pluto at approximately 30 AU, and beyond. At the time of this analysis, SDC has reported measurements out to approximately 20 AU. For Pioneer 10, it is important to note that the instrument originally had two redundant meteoroid sensors; however, one entire sensor failed just weeks after launch [*Humes*, 1980]. Following the reasoning of *Landgraf et al.* [2002], we have confidence in the results reported by Pioneer 10.

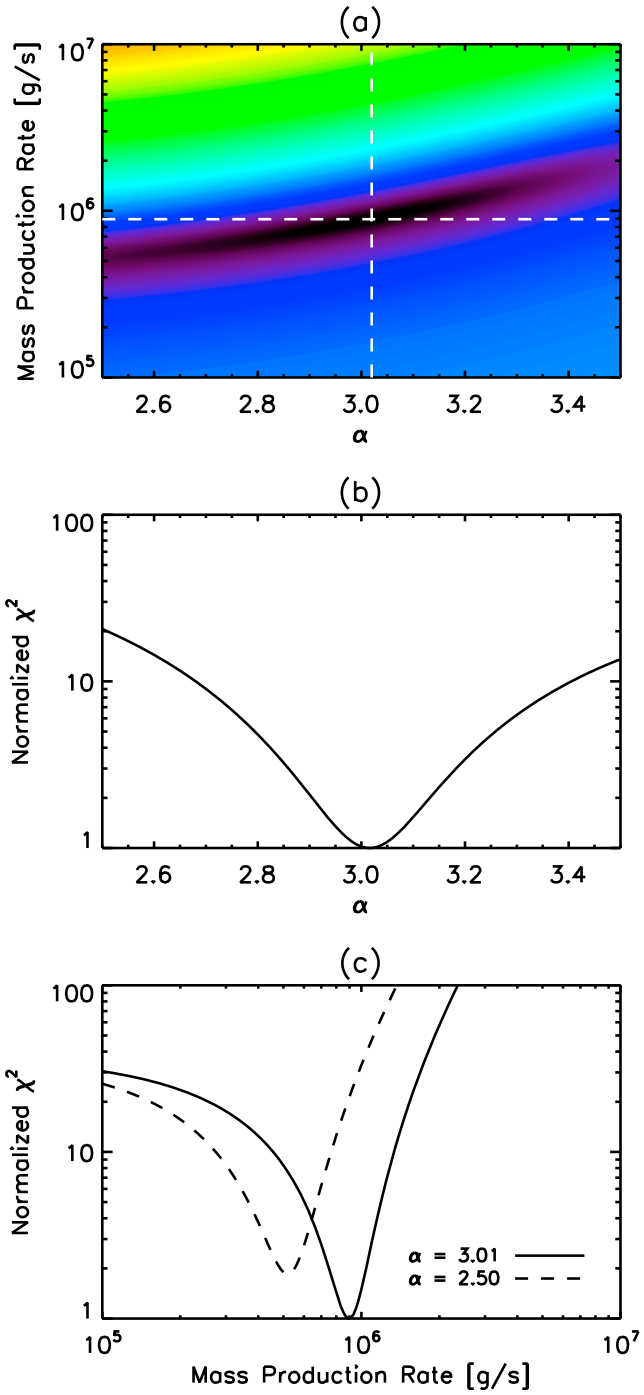

Figure 2. (a) The $\log_{10}\chi^2$ goodness-of-fit parameter as a function of the mass production rate, $\dot{M}$, and the power law exponent, α, where warm colors indicate higher $\log_{10}\chi^2$ values and colder colors indicate lower $\log_{10}\chi^2$ values. The two dashed white lines indicate the mass production rate and power law exponent corresponding to the minimum χ^2 value. (b) χ^2 trace as a function of the power law exponent, α, along the minimum mass production rate. (c) χ^2 trace as a function of the mass production rate, $\dot{M}$, along the minimum power law exponent. Also shown as the dotted line is the χ^2 trace as a function of $\dot{M}$ for $\alpha = 2.5$.

[9] In order to convert the measured fluxes into densities, the dust grain impact velocity must be calculated as a function of heliocentric distance. To calculate the dust grain impact velocity onto each instrument, we subtracted the spacecraft velocity from the local dust grain velocity for grains on circular orbits, including the effect of solar radiation pressure. In order to check the validity of the assumption of circular orbits, we also used the position and velocity information from the model to compute impact velocities for individual dust grain trajectories that crossed the New Horizons and Pioneer 10 trajectories. This analysis showed that while the presence of slightly non-circular orbits does cause the impact velocity of any individual grain to be above or below the local circular impact speed, it does not cause a significant bias in average grain impact speeds.

3.2. Comparison to Model

[10] Having established both model-predicted relative densities for each radius bin and cumulative density measurements for both spacecraft, we can now establish overall dust production parameters for the EKB. In order to provide the best comparison to previous theoretical calculations [*Stern*, 1996; *Yamamoto and Mukai*, 1998], we assume that global dust production in the EKB is described by a power-law distribution in mass, $d\dot{M}/dm = \dot{M}_o(m/m_o)^{-\alpha/3}$, where $d\dot{M}/dm$ is the differential mass production rate of dust grains between m and $m + dm$ in the EKB, $\dot{M}_o$ is a normalization constant and $m_o = 10^{-11}$ g. The net mass production rate in the EKB, $\dot{M}$ [g/s], is then found by integrating the distribution from $m_{\min} = 10^{-14}$ g ($a_d = 0.1$ μm) to $m_{\max} = 10^{-8}$ g ($a_d = 10$ μm). (We emphasize here that $\dot{M}$ and α do not represent the instantaneous mass distribution at any specific point in the solar system, but rather the overall production of grains summed over the EKB.) To determine the best-fit $\dot{M}$ and α, we vary the two parameters over a wide range and for each pair of $[\dot{M}, \alpha]$, first calculate a model-predicted cumulative density for both SDC and Pioneer 10 along their trajectories from each instrument's minimum threshold up to $a_d = 10$ μm by co-adding the relative densities for each size bin according to the power-law distribution. We then calculate a two-parameter χ^2 goodness-of-fit function between the model-predicted densities and the in-situ measurements, with each measurement inversely weighted by its respective error [*Press et al.*, 2007]. SDC and Pioneer 10 χ^2 values are computed separately and combined with equal weight.

[11] Figure 2a shows the relative $\log_{10}\chi^2$ value as a function of both the mass production rate, $\dot{M}$, and the power law index, α. The minimum χ^2 value occurs at $\dot{M} = (8.9 \pm 0.5) \times 10^5$ g/s and $\alpha = 3.02 \pm 0.04$, with the mass production rate well within previous theoretical estimates [*Stern*, 1996; *Yamamoto and Mukai*, 1998]. The error bars represent a 10% deviation in χ^2 along the associated minimum contour. Figures 2b and 2c show the χ^2 contours along each of the minimum values for both $\dot{M}$ and α, respectively, demonstrating that the fits for both parameters are robust. Previous work has typically assumed a power law index of $\alpha = 2.5$ [*Moro-Martin and Malhotra*, 2003; *Kuchner and Stark*, 2010], which can be compared with this work using Figure 2c. Along the $\alpha = 2.5$ contour, the associated minimum mass production rate is approximately 5.2×10^5 g/s,

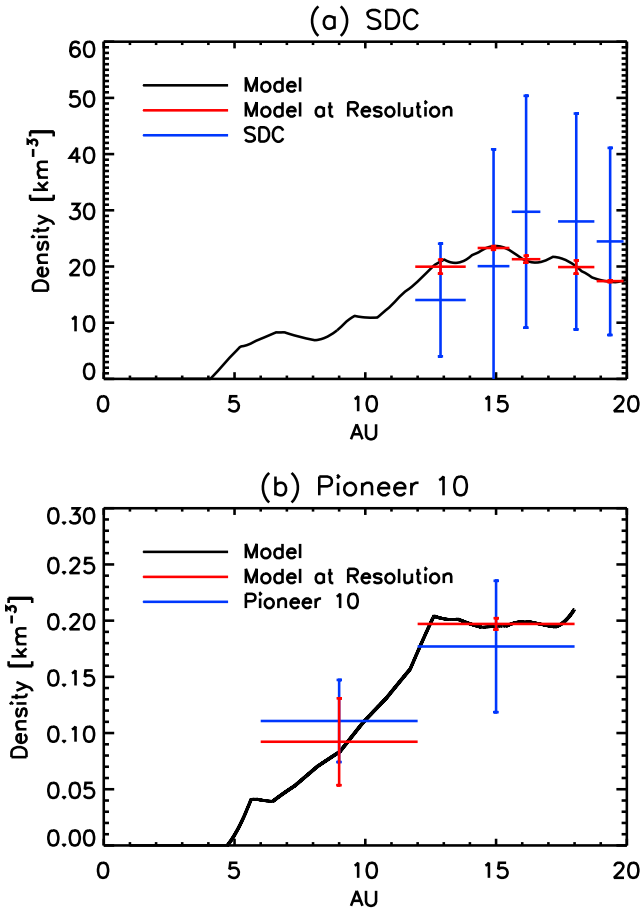

Figure 3. A comparison of the model-predicted densities along the trajectories of (a) SDC and (b) Pioneer 10 using the best fit mass production rate and power law exponent. The solid black line is the model-predicted density along each spacecraft's trajectory, the blue points are the respective instrument measurements and the red points are the model densities averaged over the respective instrument's spatial resolution, for comparison.

slightly lower than the optimal value computed here. Using the best-fit values for the mass production rate and the power law index, the model predicted densities can be compared with the experimental observations. Figure 3 shows the model and experimental densities as a function of heliocentric distance for both SDC and Pioneer 10. For both instruments, the model predicts densities within the reported experimental errors.

4. Significance and Future Work

[12] The use of both Pioneer 10 and Student Dust Counter measurements of interplanetary dust density in the outer solar system at two differing grain radii has allowed us to place tighter constraints on the mass production rate and power-law exponent for grains produced in the Edgeworth-Kuiper Belt. The best-fit mass production value agrees well with previous theoretical estimates [*Stern*, 1996; *Yamamoto and Mukai*, 1998], although we calculate a somewhat steeper mass distribution than is typically assumed. These values, in combination with the results of the grain-tracing model, can be used to compute the incoming velocity distributions and differential flux of interplanetary grains to the giant planets, which may vary as a function particle size and heliocentric distance. In turn, this information can be used to increase the precision of estimates of several phenomena in the outer solar system, as described in Section 1. Future work will include analysis of the size distributions at instantaneous heliocentric points (similar to *Moro-Martin and Malhotra* [2003]), use SDC measurements to further constrain dust production parameters in the EKB and search for evidence of MMR with Neptune in the outer solar system. The effect that other important phenomena, such as solar wind sputtering, sublimation and grain-grain collisions, or the presence of other dust grain sources, may have on the dust grain-tracing model is also future work.

[13] **Acknowledgments.** The authors acknowledge initial code development efforts by Mr. D. Steussy, who was supported by NASA's OPR Program (NNG06GF48G). This work was also supported by the NASA New Horizons mission. The authors also wish to thank N. Altobelli and another anonymous reviewer for helpful comments which greatly improved the paper.

[14] The Editor thanks Nicolas Altobelli and an anonymous reviewer for their assistance in evaluating this paper.

References

Burns, J. A., et al. (1979), Radiation forces on small particles in the solar system, *Icarus*, *40*, 1–48.

Burns, J. A., et al. (1999), The formation of Jupiter's faint rings, *Science*, *284*, 1146–1150.

Chambers, L. S., et al. (2008), Hydrodynamical and radiative transfer modeling of meteoroid impacts into Saturn's rings, *Icarus*, *194*, 623–635.

Colwell, J. E., and L. W. Esposito (1990), A numerical model of the Uranian dust rings, *Icarus*, *86*, 530–560.

Cuzzi, J. N., and P. R. Estrada (1998), Compositional evolution of Saturn's rings due to meteoroid bombardment, *Icarus*, *132*, 1–35.

Durisen, R. H., et al. (1989), Ballistic transport in planetary ring systems due to particle erosion mechanisms: I. Theory, numerical methods and illustrative examples, *Icarus*, *80*, 136–166.

Durisen, R. H., et al. (1992), Ballistic transport in planetary ring systems due to particle erosion mechanisms: II. Theoretical models for Saturn's A- and B-ring inner edges, *Icarus*, *100*, 364–393.

Durisen, R. H., et al. (1996), Ballistic transport in planetary ring systems due to particle erosion mechanisms: III. Torques and mass loading by meteoroid impacts, *Icarus*, *124*, 220–236.

Feuchtgruber, H., et al. (1997), External supply of oxygen to the atmospheres of the giant planets, *Nature*, *389*, 159–162.

Gustafson, B. A. S. (1994), Physics of zodiacal dust, *Annu. Rev. Earth Planet. Sci.*, *22*, 553–595.

Holmes, E. K., et al. (2003), Resonant structure in the Kuiper Belt: An asymmetric Plutino disk, *Astrophys. J.*, *597*, 1211–1236.

Horányi, M. (1996), Charged dust dynamics in the solar system, *Annu. Rev. Astron. Astrophys.*, *34*, 383–418.

Horányi, M., et al. (2008), The Student Dust Counter on the New Horizons Mission, *Space Sci. Rev.*, *140*, 387–402.

Humes, D. H. (1980), Results of Pioneer 10 and 11 meteoroid experiments: Interplanetary and near-Saturn, *J. Geophys. Res.*, *85*(A11), 5841–5852.

Jewitt, D. C., and J. X. Luu (1995), The solar system beyond Neptune, *Astron. J.*, *109*, 1867–1876.

Kavelaars, J. J., et al. (2009), The Canada-France Ecliptic Place Survey—L3 data release: The orbital structure of the Kuiper Belt, *Astron. J.*, *137*, 4917–4935.

Krivov, A. V., et al. (2003), Impact-generated dust clouds around planetary satellites: Spherically symmetric case, *Planet. Space Sci.*, *51*, 251–269.

Kuchner, M. J., and C. C. Stark (2010), Collisional grooming models of the Kuiper Belt dust cloud, *Astron. J.*, *140*, 1007–1019.

Landgraf, M. (2000), Modeling the motion and distribution of interstellar dust inside the heliosphere, *J. Geophys. Res.*, *105*(A5), 10,303–10,316.

Landgraf, M., et al. (2002), Origins of solar system dust beyond Jupiter, *Astron. J.*, *123*, 2857–2861.

Liou, J.-C., and H. A. Zook (1997), Evolution of interplanetary dust particles in mean motion resonances with planets, *Icarus*, *128*, 354–367.

Liou, J.-C., and H. A. Zook (1999), Signatures of the giant planets imprinted on the Edgeworth-Kuiper Belt dust disk, *Astron. J.*, *118*, 580–590.

Liou, J.-C., et al. (1995), Radiation pressure, Poynting-Robertson drag, and solar wind drag in the restricted three-body problem, *Icarus*, *116*, 186–201.

Luu, J. X., and D. C. Jewitt (2002), Kuiper Belt objects: Relics from the accretion disk of the Sun, *Annu. Rev. Astron. Astrophys.*, *40*, 63–101.

Molina-Cuberos, G. J., et al. (2001), Ionospheric layer induced by meteoritic ionization in Titan's atmosphere, *Planet. Space Sci.*, *49*, 143–153.

Moro-Martin, A., and R. Malhotra (2002), A study of the dynamics of dust from the Kuiper Belt: Spatial distribution and spectral energy distribution, *Astron. J.*, *124*, 2305–2321.

Moro-Martin, A., and R. Malhotra (2003), Dynamical models of Kuiper Belt dust in the inner and outer solar system, *Astrophys. J.*, *125*, 2255–2265.

Moses, J. I. (1992), Meteoroid ablation in Neptune's atmosphere, *Icarus*, *99*, 368–383.

Nesvorný, D., et al. (2010), Cometary origin of the zodiacal cloud and carbonaceous micrometeorites: Implications for hot debris disks, *Astrophys. J.*, *713*, 816–836.

Northrop, T. G., and J. E. P. Connerney (1987), A micrometeorite erosion model and the age of Saturn's rings, *Icarus*, *70*, 124–137.

Parker, E. N. (1958), Dynamics of the interplanetary gas and magnetic fields, *Astrophys. J.*, *128*, 664–676.

Poppe, A., and M. Horányi (2011), The effect of Nix and Hydra on the putative Pluto-Charon dust cloud, *Planet. Space Sci.*, *59*, 1647–1653.

Poppe, A., D. James, B. Jacobsmeyer, and M. Horányi (2010), First results from the Venetia Burney Student Dust Counter on the New Horizons mission, *Geophys. Res. Lett.*, *37*, L11101, doi:10.1029/2010GL043300.

Press, W. H., et al. (2007), *Numerical Recipes: The Art of Scientific Computing*, 3rd ed., Cambridge Univ. Press, New York.

Stern, S. A. (1996), Signatures of collisions in the Kuiper Disk, *Astron. Astrophys.*, *310*, 999–1010.

Stern, S. A. (2008), The New Horizons Pluto Kuiper Belt Mission: An overview with historical context, *Space Sci. Rev.*, *140*, 3–21.

Thiessenhusen, K.-U., et al. (2002), A dust cloud around Pluto and Charon, *Planet. Space Sci.*, *50*, 79–87.

Verbischer, A. J., et al. (2009), Saturn's largest ring, *Nature*, *461*, 1098–1100.

Vitense, C., et al. (2010), The Edgeworth-Kuiper debris disk, *Astron. Astrophys.*, *520*, A32.

Yamamoto, S., and T. Mukai (1998), Dust production by impacts of interstellar dust on Edgeworth-Kuiper Belt objects, *Astron. Astrophys.*, *329*, 785–791.

E. Grün, D. Han, M. Horányi, and M. Piquette, Laboratory for Atmospheric and Space Physics, University of Colorado at Boulder, UCB 590, Boulder, CO 80309, USA.

A. R. Poppe, Space Sciences Laboratory, University of California, 7 Gauss Way, Berkeley, CA 94720, USA. (poppe@ssl.berkeley.edu)